Magnetism in dilute magnetic oxide thin films based on SnO_2

C. B. Fitzgerald, M. Venkatesan, L. S. Dorneles, R. Gunning, P. Stamenov, and J. M. D. Coey
School of Physics, Trinity College, Dublin 2, Ireland

P. A. Stampe and R. J. Kennedy
Department of Physics, Florida A&M University, Tallahassee, Florida 32307, USA

E. C. Moreira
Centro Universitario Franciscano, 97010-032, Santa Maria-RS, Brazil

U. S. Sias
Instituto de Fisica, Universidade Federal do Rio Grande do Sul, 91501-970, Porto Alegre-RS, Brazil
(Received 24 October 2005; revised manuscript received 16 March 2006; published 12 September 2006)

Thin films of SnO_2 prepared by pulsed-laser deposition on R-cut sapphire substrates exhibit ferromagnetic properties at room temperature when they are doped with Cr, Mn, Fe, Co, or Ni, but not with other 3*d* cations. Extrapolated Curie temperatures are generally in excess of 500 K. The moment of the films is roughly independent of doping level, from 0.1–15 at. %, with a value per unit substrate area of 200 ± 100 μ_B nm^{-2}. When magnetization is expressed as a moment per 3*d* dopant ion, it varies from more than the spin-only value at low concentrations to less than 0.2 μ_B/ion near the percolation threshold. Greatest values are found for iron. The magnetization of the films is highly anisotropic with values when the field is applied perpendicular to the substrate more than double the in-plane values. There is little hysteresis except at high doping levels. The oxides are degenerate *n*-type semiconductors with a Hall mobility of 100 cm^2 V^{-1} s^{-1} and 1.4×10^{19} carriers cm^{-3} in a one-band model, but no anomalous Hall effect or magnetoresistance was observed at room temperature. The data are discussed in relation to (a) the donor impurity-band model of ferromagnetism in semiconductors and (b) the magnetic defect model.

DOI: 10.1103/PhysRevB.74.115307 PACS number(s): 75.50.Pp, 73.43.Qt, 74.25.Gz

I. INTRODUCTION

Over the past four years, there have been many reports on ferromagnetism above 300 K in thin films of wide-gap semiconductors doped with a few percent of 3*d* transition-metal ions. The materials are oxides—TiO_2,[1,2] ZnO,[3–7,12] SnO_2,[8–12] or nitrides—GaN,[13] AlN [14]. The 3d dopants are Sc, Ti, V, Cr, Mn, Fe, Co, or Ni. There is a recent review of results in ZnO and GaN by Liu *et al.*[15]

High-temperature ferromagnetism was completely unexpected in these hosts because the magnetic doping level x, defined as the fraction of cations which are 3*d* transition metals, lies far below the percolation threshold, x_p, needed for long-range order based on superexchange or double exchange interactions. In some cases x can be as low as 1–2 %.[1,16] Furthermore these ferromagnets are usually *n* type, unlike the well-studied III-V semiconductors such as $(Ga_{1-x}Mn_x)As$, which are *p* type, and show Curie temperatures of up to 170 K in thin films with $x=8\%$.[17] Exchange in that case is mediated by holes in the As 4*p* band which are created by the Mn doping. Moreover, it is known that the *pd* exchange coefficient β is several times greater than the *sd* exchange coefficient α,[18] so *n*-type dilute magnetic semiconductors with smaller doping would not have been expected to order magnetically at temperatures above 50 K. Even when a mechanism for long-range exchange coupling exists, the high Curie temperatures are baffling. No ferromagnet has a higher T_c than cobalt (1390 K). The Curie temperature scales as x or $x^{1/2}$ in theories of dilute ferromagnetism[19,20] so it seems that a Curie temperature well in excess of 300 K should be impossible in a uniform sample with $x=5\%$, for example.

The reports of high Curie temperatures were therefore greeted with scepticism, and the belief that the data somehow reflect the presence of impurity phases, rather than the intrinsic behavior of the dilute magnetic oxide or nitride. For example, the first report of high temperature ferromagnetism in a dilute magnetic oxide was for Co-doped TiO_2 (anatase) by Matsumoto *et al.*,[1] for which $T_C>300$ K was reported for 1–2 % doping. Subsequent examination of samples of TiO_2 revealed the presence of clusters of metallic cobalt,[21] which were at least partially-responsible for the observed ferromagnetism and magnetotransport properties.[22] But other samples of Co-doped TiO_2, however, have been shown to be ferromagnetic and free of cobalt clusters.[23] In systems such as ZnO doped with Co for example, which exhibit an extended range of solid solubility in reducing conditions,[24] no secondary phases have been found, at least in dilute thin films prepared at high temperature and in a low pressure of oxygen.[25,26] Furthermore, there is spectroscopic evidence in that case that Co^{2+} does occupy tetrahedral cation sites in the wurtzite structure.[26–30]

The first report of high-temperature ferromagnetism in SnO_2 films was by Ogale *et al.*,[8] who reported a Curie temperature $T_c=650$ K in a cobalt-doped thin film sample with $x=5\%$, and an astonishingly large moment of 7.5 μ_B per cobalt ion. High temperature ferromagnetism was subsequently reported for $(Sn_{1-x}Fe_x)O_2$ with $x=14\%$ (Ref. 9) and $x=0.5$–5 %,[44] $(Sn_{1-x}Cr_x)O_2$ with $x=5\%$,[10] $(Sn_{1-x}V_x)O_2$ with

$x=7\%$,[11] and $(Sn_{1-x}Ni_x)O_2$ with $x=5\%$,[12] but the Mn-doped material was found to be paramagnetic down to 5 K.[31] Ferromagnetism in the *V*-doped films depends on the nature of the substrate on which they are deposited.[11] Hong *et al.* found moments as high as 3.0 μ_B per vanadium ion for films on $LaAlO_3$.

Up to now, a systematic study of the high temperature ferromagnetism as a function of cation-doping x, or the nature of the transition-metal cation M has been carried out for ZnO.[4] Most other investigations have been for a single dopant and a few compositions. There is often little agreement between the results obtained in different laboratories. A plot of all measurements of the average cation moment m versus x for the widely studied $(Zn_{1-x}M_x)O$ system for example, shows scattered values, with no discernable trend.[20] We have therefore undertaken another systematic investigation of the magnetic and transport properties of a dilute magnetic semiconductor system over a wide range of doping. The $(Sn_{1-x}M_x)O_2$ system was chosen because the SnO_2 films can be doped with all the 3*d* transition metal ions, and it is possible to produce uniform thin films with $M=$Mn, Fe, or Co over a wide range of composition $0.1<x<30\%$. Our aim was to develop some understanding of the ferromagnetism in these remarkable *n*-type transparent conducting oxides.[32] The results are first discussed in terms of carrier-mediated exchange in a spin-split impurity band derived from bound magnetic polarons,[33] or in a spin-split 4s/5s conduction band, and then in terms of a model of ferromagnetic ordering of moments of molecular orbitals with 2*p* hole character, which may be associated with defects in the interface region.

II. EXPERIMENTAL METHODS

The oxide films were prepared by pulsed-laser deposition (PLD). Ceramic targets $(Sn_{1-x}M_x)O_2$, with $0.001<x<0.05$, were synthesized from stoichiometric amounts of high purity 99.99% SnO_2 and MO ($M=$Mn, Fe, Co) powders. In addition a series of ten $(Sn_{0.985}M_{0.015})O_2$ targets was prepared, where $M=$Sc-Zn. The oxide powders were thoroughly ground under isopropanol, then pressed into pellets and sintered at 1150 °C for 24 h. The structural and magnetic characteristics of the targets have been reported elsewhere.[34] Minor amounts of secondary phases were found in the targets—$SnCo_2O_4$ and α-Fe_2O_3 in the Co and Fe doped samples, respectively. The ceramics with $M=$Mn or Fe were ferromagnetic, with small room temperature saturation magnetisation values of 0.2 and 1.8 A m^2 Kg^{-1} for $Sn_{0.95}Mn_{0.05}O_2$ and $Sn_{0.95}Fe_{0.05}O_2$, respectively. Corresponding moments are 0.1 μ_B/Mn and 1.0 μ_B/Fe, respectively. The Co-doped targets show no ferromagnetism down to 5 K.[34]

Following Ogale *et al.*,[8] the thin films were deposited on *R*-cut $(1\bar{1}02)$ sapphire substrates using a KrF excimer laser operating at 248 nm and 10 Hz. Laser fluence on the target was 1.8 J cm^{-2}. The target-substrate distance was 35 mm and the oxygen pressure was 10^{-4} mbar. The substrate temperature was 750 °C. Film thickness was determined after deposition by small angle x-ray scattering and it was also monitored during deposition using optical reflectivity at 635 nm. Independent thickness measurements were made by atomic force microscopy (AFM) of a trench milled by argon-ion etching, and by direct observation of a cross section in the transmission electron microscope. A typical deposition rate was 10 nm/min, with the laser operating at 10 Hz.

Crystal structure measurements were performed using a Philips PW3040 four-circle materials research x-ray diffractometer. This allowed the measurement of off-axis as well as on-axis scans in SnO_2 films doped with V, Cr, or Mn. In-plane and out-of-plane orientation, mosaicity and lattice parameters for each film were determined using $\theta/2$ scans, rocking curves, area maps, and pole figure measurements. The thin-film optics on this diffractometer do not allow high-resolution measurements—a minimum line width of approximately 0.4° is observable for the (400) reflection of a (100) oriented single crystal silicon wafer. The determination of crystallite size through line width is thus impossible. However, line width from film to film can be compared to give relative mosaicities and a measure of the relative quality of the films. Small-angle measurements were performed using a Philips X'Pert PRO x-ray diffractometer with enhanced optics—a minimum line width of approximately 0.06° is observable for the (400) reflection of a (100) oriented single crystal silicon wafer.

Scanning electron microscopy (SEM), with energy dispersive x-ray analysis (EDAX) was used for elemental analysis and mapping. Rutherford backscattering spectroscopy (RBS) was employed to determine the chemical composition of the SnO_2 films doped with Fe. The samples were analyzed by means of a 2.0 MeV $^4He^+$ incident beam and the backscattered particles were detected by a Si(Li) surface barrier detector placed at 165° with respect to the incident beam direction.

Root mean square surface roughness was determined by atomic force microscopy (AFM) and magnetic contrast was recorded using magnetic force microscopy (MFM). Magnetization measurements were made in a SQUID magnetometer at both 300 K and 5 K. Curie temperatures (T_c) were measured using a SQUID magnetometer with a high temperature furnace in a field of 150 mT. The ^{57}Fe Mössbauer spectra were collected at room temperature and at 16 K in transmission geometry with a ^{57}Co (Rh) source, as reported previously.[9,34]

Optical spectra were recorded at room temperature in the range 2–6 eV using a Perkin Elmer dual-beam spectrophotometer. Resistivity measurements were carried out by the standard van der Pauw technique in the temperature range 5–300 K using Au/In contacts. Magnetoresistance was measured in a Quantum Design 14 Tesla PPMS system.

III. RESULTS

A. Film composition and structure

A typical film thickness was 90 nm. The different methods of measuring film thickness consistently agreed to within ±5%. Films were smooth and featureless in SEM, with no evidence of the droplets sometimes seen in films produced by PLD. In TEM the 65 nm Mn-doped film shows peak-to-peak surface undulation of 1.5 nm. AFM images of a thick

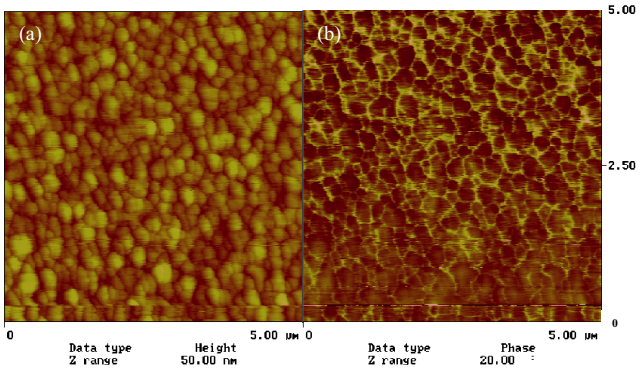

FIG. 1. (Color online) (a) Atomic force microscope image of a film of composition $(Sn_{0.75}Fe_{0..25})O^2$ and (b) magnetic force microscope image of the same area, corrected for surface topology.

(240 nm) $Sn_{0.75}Fe_{0.25}O_2$ film show a blister-like surface topology with rms roughness of 5 nm [Fig. 1(a)].

The compositions of the films are very different from those of the ceramic targets from which they are made. The nominal composition x' is plotted against the measured composition x, determined by EDAX analysis, in Fig. 2 for the $(Sn_{1-x}M_x)O_2$ series, where M=Mn,Fe,Co. Pulsed-laser deposition does not maintain the stoichiometry of the target in face of the volatility of SnO_2, which is resputtered from the growing film. In fact the films contain roughly *four* times as much of the 3*d* element as the targets. A lesser enhancement of 3*d* dopant concentration has been reported in PLD ZnO films doped with Co or other transition metals.[16,35]

The compositional uniformity was investigated in Fe-doped SnO_2 films using RBS spectroscopy, the spectra being analyzed using the RUMP program.[36] An RBS spectrum of a 150 nm Fe-doped SnO_2 film produced from an $Sn_{0.97}Fe_{0.03}O_2$ target is shown in Fig. 3 where the edges for each element are indicated by arrows. It can be noted that the Sn peak and the dopant peak are well separated. The uniform composition of the film is evidenced by the symmetry of the

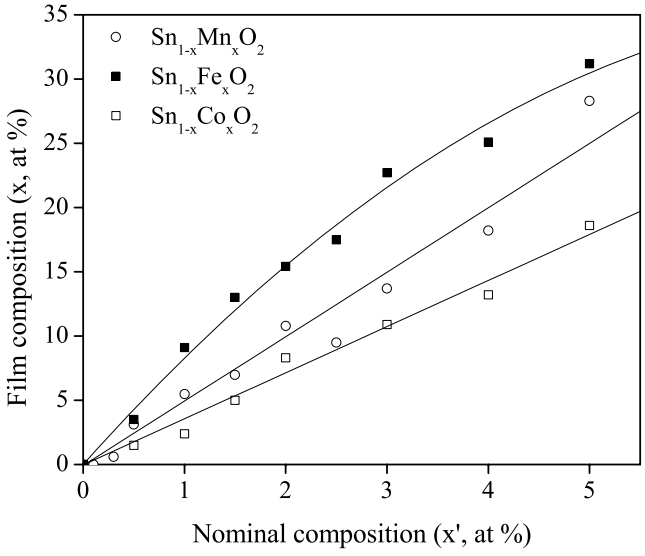

FIG. 2. Plot of the composition of the film x versus the nominal composition of the target determined by EDAX measurements.

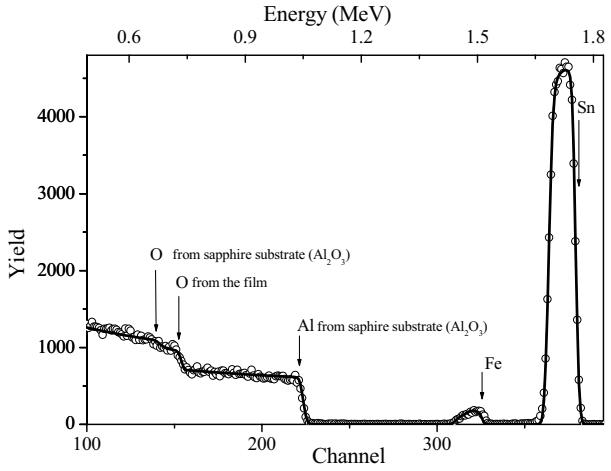

FIG. 3. RBS spectra (dots) of film grown from $(Sn_{0.97}Fe_{0.03})O_2$. Line shows the simulation using the RUMP program.

Sn peak. The Fe concentration obtained from the fit in Fig. 3 is 12 at. % at the surface but it drops to a lower value towards the film-substrate interface. A cross section of a $Sn_{0.94}Mn_{0.06}O_2$ thin film was examined by scanning transmission electron microscopy. No appreciable compositional variation was found across the 65 nm film.

An x-ray diffraction pattern is shown in Fig. 4 for a typical, cobalt doped, film on *R*-cut sapphire. The full width at half maximum (FWHM) from rocking curve measurements is 0.6° for a 150 nm thick $Sn_{0.93}Co_{0.07}O_2$ film, similar to previous reports on CVD films.[37] For all the other dopants, the width of the rocking curve is between 0.6 and 0.8°, with the exception of Cr, for which the width was 1.3°. There is a strong (101) texture, with no evidence of secondary phases except for an unidentified peak at 2θ=145.5° in a few of the Mn-doped films. From these data, we can only obtain the d_{101} lattice spacing, which is plotted as a function of composition in Fig. 5. The bulk value of d_{101} for SnO_2 is 2.64 Å, so the films are dilated perpendicular to the plane of the substrate. The strain does not vary with film thickness, as indicated as the insert to Fig. 5.

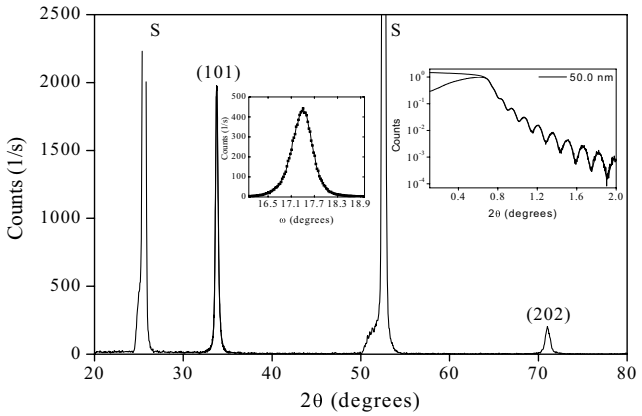

FIG. 4. X-ray diffraction pattern for a thin film of $(Sn_{0.93}Co_{0.07})O_2$. One insert shows the rocking curve with a FWHM of 0.6°. The second insert shows the small angle x-ray scattering and simulation for a 50 nm cobalt-doped film.

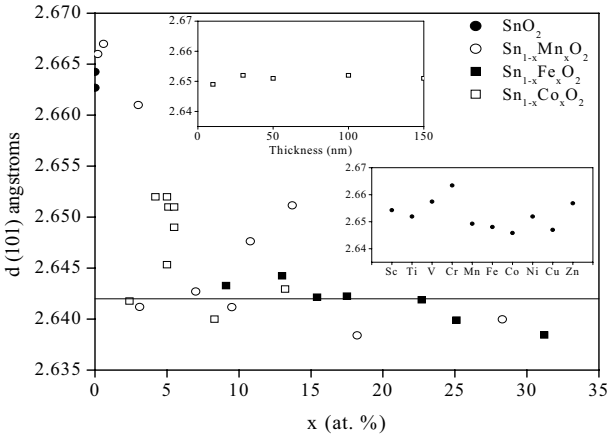

FIG. 5. The d_{101} lattice spacing for $(Sn_{1-x}M_x)O_2$ films with M=Mn, Fe, Co—the solid line indicates the value for bulk SnO_2. The first insert displays the variation of the d_{101} spacing as a function of film thickness in a series of $Sn_{0.95}Co_{0.05}O_2$ thin films, while the second shows how d_{101} varies with transition metal dopant at a nominal doping level of x=0.05.

A full set of lattice parameters was obtained for SnO_2 films doped with V, Cr, or Mn, using least-squares fits to a triclinic cell of the position of 18 off-axis reflections. The values are the same within 2%, and show that the films are indeed distorted from tetragonal. For the chromium-doped film (uncertainty shown in brackets) a=4.720(2), b=4.715(4), c=3.193(2), α=90.03(4)°, β=89.09(5)°, γ=90.00(4)°.

The pole figure for the {101} family of planes of a chromium-doped film is shown in Fig. 6. There are two orientations present, but one orientation is much stronger than the other. Similar results are observed for films doped with V or Mn. The two orientations differ only by an 180° in-plane rotation, and both could be expected to be present due to the twofold symmetry of the R-plane sapphire surface. The conclusion is that the films are highly oriented.

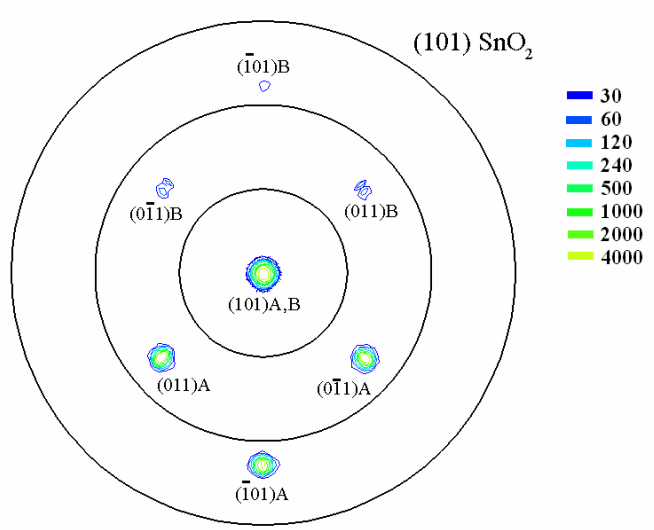

FIG. 6. (Color online) Pole figure of the {101} family of planes for a thin film of $(Sn_{0.96}Cr_{0.04})O_2$.

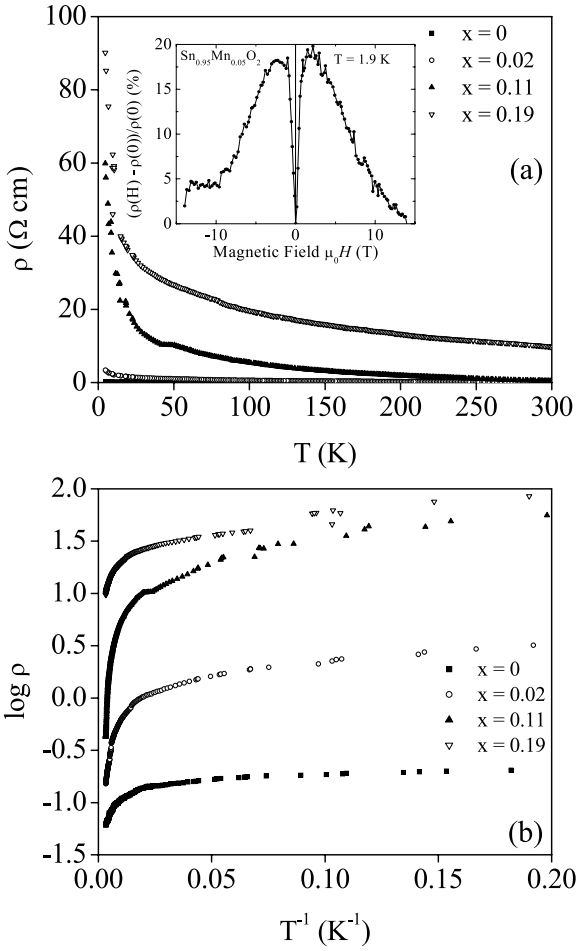

FIG. 7. Resistivity of the $(Sn_{1-x}Co_x)O_2$ series plotted (a) on a linear scale and (b) on a logarithmic scale versus $1/T$.

B. Electrical and electronic properties

The electrical conductivity of the end member is that of a degenerate n-type semiconductor (Fig. 7). Resistivity at room temperature is 7.2 mΩ cm, and the activation energy at low temperatures is only 0.2 meV. The Hall coefficient R_H=4.3 $\Omega m\,T^{-1}$, yields a carrier concentration n_e of 1.4×10^{25} m^{-3} in a one-band model, and a mobility of 100 $cm^2\,V^{-1}\,s^{-1}$. For comparison, the apparent carrier concentration in a 4% Co-doped film is 1.2×10^{24} m^{-3} at 100 K. Hall voltage was dominated by magnetoresistance contributions below 100 K. No anomalous Hall effect was observed. The cation density in SnO_2 is 2.8×10^{28} m^{-3}, so the electronic doping level δ is 0.05%. On increasing x, the oxides become progressively more resistive (Fig. 7). With Co doping films are conducting for all values of x, but films with $x>15\%$ for Fe or $x>7\%$ for Mn have a resistance greater than 40 MΩ. The films doped with Cr or Ni are insulating.

The magnetoresistance measured at 1.9 K for $Sn_{0.95}Mn_{0.05}O_2$ film is shown as inset in Fig. 7. The magnetoresistance ratio at 1.9 K is about 18%. The resistance has an initial positive, quadratic variation with field while saturating in about 2 Tesla. In higher fields, there is a slowly-saturating negative term, which may be due to ionized impurity scattering. This behavior can be attributed to the standard

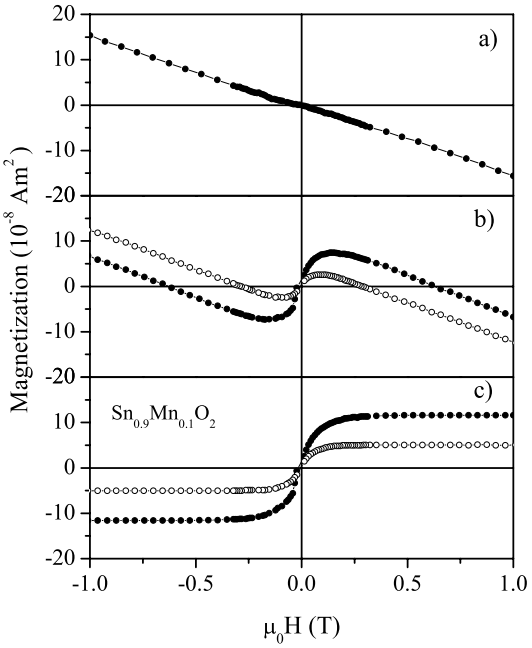

FIG. 8. Magnetization curves of films grown from (a) SnO_2 and (b) from $Sn_{0.98}M_{0.02}O_2$ targets. Data for the Mn-doped are shown for the field applied parallel (○) and perpendicular (●) to the plane of the substrate. The magnetism of the film after correcting for the sapphire substrate signal is indicated in the panel (c)

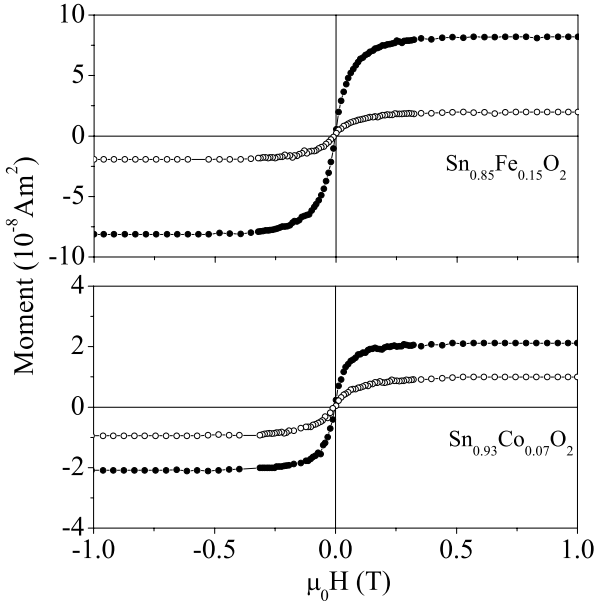

FIG. 9. Magnetization curves for thin films of $(Sn_{1-x}M_x)O_2$ with M=Fe or Co, measured with the field applied parallel (○) and perpendicular (●) to the film plane.

two-band picture with a possible weak localization contribution below 20 K. No measurable magnetoresistance is observed above 100 K. The cobalt-doped film was too resistive to measure at 1.9 K.

Optical absorption spectra for SnO_2 pure and doped films show a broad absorption edge at 330 nm (3.8 eV), corresponding to the band gap.

C. Magnetic properties

Magnetization curves were measured for all samples at 5 K and at 300 K in the SQUID magnetometer. Data are corrected for the diamagnetism of the substrate, which gives a slope of -1.8×10^{-7} A m^2 T^{-1}. Some representative results are presented in Fig. 8. Figure 8(a) shows the diamagnetic signal measured for the substrate with an undoped SnO_2 film. Figure 8(b) shows magnetization measured on a $(Sn_{0.90}Mn_{0.10})O_2$ film. There is a remarkable difference when the field is applied parallel or perpendicular to the film plane. This anisotropy varies from sample to sample, but the magnetic moment at saturation can be as much as four times greater when the field is applied perpendicular to the film plane than it is in the parallel direction. The SQUID magnetometer was calibrated separately for the two directions using a film of Fe_3O_4. The calibration constant was 19% smaller for the parallel orientation than for the perpendicular orientation. It must be remembered that the mass of the substrate is typically one thousand times greater than that of the film, so the procedure for data reduction whereby the diamagnetic contribution of the substrate is determined by the slope from 3 to 5 T does not allow any high field slope of the film magnetization in this region to be determined.

Figure 9 presents data on Co and Fe doped SnO_2 films deposited from $Sn_{0.98}M_{0.02}O_2$ targets, which show similar anisotropy to the Mn-doped films. For all films, the magnetisation curves at 5 K differed by less than 10% from those measured at room temperature, from which we infer that the Curie temperatures (T_c) are well above room temperature in all samples. T_c was measured directly from a thermal scan in one case, an Fe-doped sample with x=14%, and it was found to be 610 K.[9]

Particularly interesting is the plot of magnetization expressed as moment per transition-metal cation in Fig. 10. Despite the scatter, there is a distinct trend. The moment increases steadily as x is reduced, reaching values comparable to, or even exceeding the free-ion spin only values when $x<0.02$. The moment becomes small ($<0.2\ \mu_B$) beyond the percolation threshold, which is x_p=0.25 for the body-centered tetragonal rutile structure. Figure 11 shows magnetization curves for Co-doped films with x=5% of different thickness. There is no systematic thickness dependence; the film moment is very roughly $5\times10^{15}\ \mu_B$, regardless of film thickness, which corresponds to 220 μ_B nm^{-2} of substrate area.

The magnetization measurements for films doped with the series of 3d elements from Sc-Zn shows that only films containing Cr, Mn, Fe, Co, or Ni are magnetic at room temperature, with the largest moments being found for Fe (Fig. 12). All compositions with Mn, Fe, and Co dopants are ferromagnetic. Little hysteresis is observed except for the Mn compound with x=28% and for the Fe compounds with $x>13\%$. A typical value of coercivity for the lower-doped films is H_c=4 kA m^{-1} with a remanence ratio M_r/M_s=5%.

The magnetic contrast seen in magnetic force microscopy (MFM), Fig. 1(b), appears to decorate the topology, consistent with uniform in-plane magnetization of the films. Both the moment and coercivity of highly Fe-doped samples were

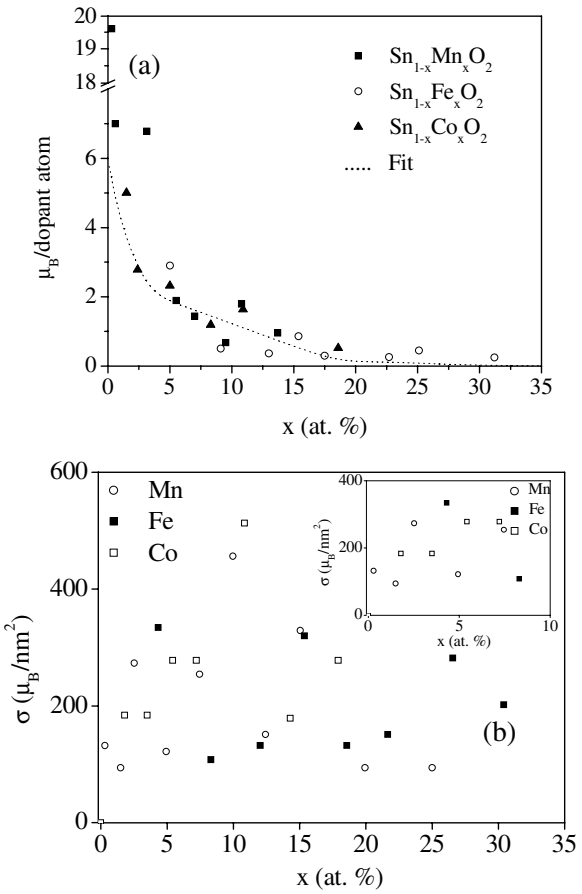

FIG. 10. (a) Magnetic moment of $(Sn_{1-x}M_x)O_2$ films, M=Mn, Fe or Co, expressed per dopant atom. (b) Magnetic moments measured on thin films of $(Sn_{1-x}M_x)O_2$ with M=Mn, Fe, or Co expressed in Bohr magnetons per unit substrate area.

stable in time, the same values were found when films were measured just after deposition as over three following years. However, the moment in the weakly-coercive Co- and Mn-doped films decays with time and diminished by a factor of ten after two years.

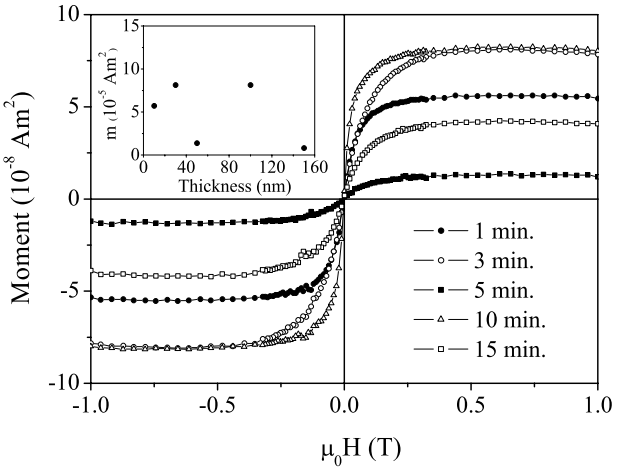

FIG. 11. Thickness dependence of the moment of $(Sn_{0.95}Co_{0.05})O_2$ films.

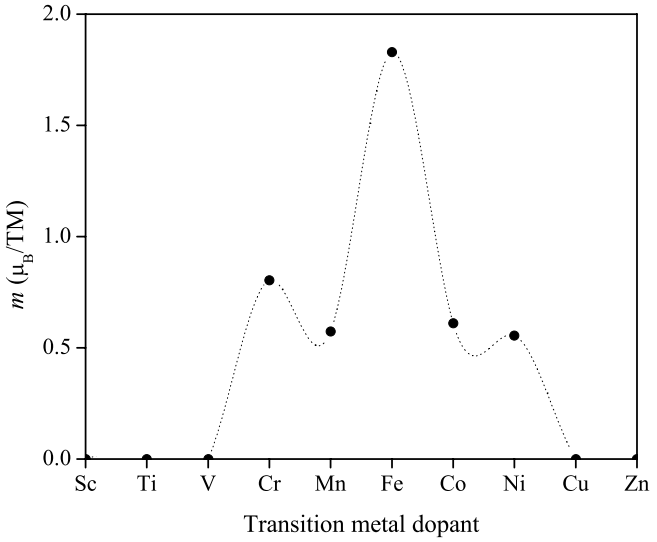

FIG. 12. Magnetic moment of $(Sn_{1-x}M_x)O_2$ films, M=Sc, Ti, …, Cu, Zn measured at room temperature with the field applied perpendicular to the film plane. The moment is expressed as μ_B/TM.

D. Mössbauer spectra

Mössbauer spectra were reported previously for a film made with $^{57}Fe_2O_3$.[9] The production method differs from that used for the films reported here insofar as Fe_2O_3 rather than FeO is used as a starting material for target preparation. Nonetheless, the spectra gives some useful insight into the magnetism. All the iron is in the ferric form in octahedral sites, with an isomer shift of 0.29 and 0.38 mm s^{-1} with respect to iron metal for paramagnetic and magnetically ordered subspectra respectively, but only 23% of the iron was magnetically ordered at room temperature in a sample with x=14%. The moment of the sample was 2.2 A m^2 kg^{-1}, which corresponds to a moment of 1.8 μ_B per ordered iron ion. The hyperfine field, 51.2 T indicates an iron moment of close to 5 μ_B. This suggests a degree of antiferromagnetic coupling among the ordered iron moments or between the iron and some magnetic defects. Other doped samples with $x>14\%$ which exhibited open hysteresis loops having $\mu_0 H_C \sim 125$ mT were found to contain most of the iron in the form Fe_3O_4 impurities.

IV. DISCUSSION

A. Charge state

The first point in a discussion of the magnetic and electric properties of these dilute ferromagnetic oxides is to try to establish the charge state of the transition-metal dopant cations. For manganese, there are three possibilities, Mn^{2+} ($3d^5$, 91 pm), Mn^{3+} ($3d^4$, 70 pm), and Mn^{4+} ($3d^3$, 52 pm). The electron configuration and ionic radius of each ion in pm is given in brackets. The most likely configuration, based on the lattice spacing data in Fig. 5 is Mn^{3+} (or possibly a mixture of Mn^{2+} and Mn^{4+}). The ionic radius of Sn^{4+} in SnO_2 is 74 pm, and the corresponding oxygen radius in the rutile structure is 135 pm. The Mn^{4+} valence state should lead to a negative strain, which is not observed.

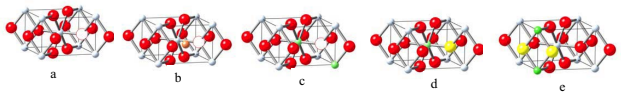

FIG. 13. (Color online) Illustration of defects in SnO_2 structure. (a) oxygen vacancy (b) oxygen vacancy and tin interstitial (c) A pair of substitutional M^{3+} cations with a oxygen vacancy (d) An substitutional M^{3+} ion with an oxygen-hole (e) A pair of M^{3+} cations with a peroxide ion.

For iron, little strain is expected because the ionic radius of Fe^{3+} is similar to that of Sn^{4+}. The data of Fig. 5 are consistent with an Fe^{3+} ($3d^5$, 67 pm) charge state, which is the one usually found in oxides. The only other possibility, Fe^{2+} ($3d^6$, 82 pm) would create a lattice dilation similar to Mn^{2+}, which is not observed (Fig. 5). Ferric iron was confirmed by the Mössbauer isomer shift and hyperfine field.[9]

As for Co, the possible charge states are Co^{2+} ($3d^7$, 82 pm) and Co^{3+} ($3d^6$, 64 pm) either of which might be in a low-spin state. The large moments at low concentrations might favor high spin Co^{3+}.

In any case, the transition-metal cations have a *lower valence than the tin for which they substitute*, so the dopants must somehow influence the defect chemistry. The isolated oxygen vacancy [Fig. 13(a)] captures an electron and forms a *F*-center deep in the gap. The doubly-occupied state *F'* lies above the conduction band edge. The defect believed to lead to conduction in SnO_2, is an oxygen vacancy associated with an interstitial tin atom [Fig. 13(b)].[33] The 8*i* octahedral interstitials at $a/2,0,c/2$ have the same multiplicity as the adjacent 8*j* tin sites. More oxygen vacancies would be introduced on doping if two Sn^{4+} ions are replaced by two M^{3+} ions together with an O^{2-} vacancy [Fig. 13(c)] rather than an interstitial Sn^{2+} ion, but such high levels of nonstoichiometry (up to 10%) are likely to destabilize the rutile lattice. Furthermore, 3*d* doping at levels $x \gg \delta$ has little influence on the conductivity of SnO_2-the doping level x has to be very much greater than the donor concentration, $\delta=0.05\%$, before the films become insulating, at least for Mn, Fe, and Co doping. The oxygen vacancies associated with the 3*d* dopants would be expected to trap the electrons which are responsible for the conductivity of SnO_2^-.

In view of the high doping levels that can be achieved in SnO_2, the defects are more likely to be electronic in nature, rather than atomic interstitials or vacancies. A suitable charge-compensating electronic defect is the replacement of a tin ion in its surrounding oxygen octahedron, $Sn^{4+}\,O^{-2}{}_6$, by $M^{3+}O^{2-}{}_5\,O^-$ [Fig. 13(d)]. The O^- ligand holes are not delocalized at the top of the oxygen 2*p* band, such as the 4*p* holes in Mn-doped GaAs for example, because the oxide becomes less conducting, not more conducting on doping. Instead, they will tend to pair up to form $O_2{}^{2-}$ peroxide ions linking adjacent octahedra, each of which is occupied by an aliovalent cation [Fig. 13(e)]. The Mn^{3+}, Fe^{3+}, and Co^{3+} levels in SnO_2 must fall in the 2*p*-5*s* gap but the M^{2+} cation levels, with an extra *d* electron, lie well above the bottom of the conduction band. An effect of doping with M^{3+} impurities is to create random spatial potential fluctuations, which tend to localize the donor electrons, whether they are in the conduction band, or in an impurity band.

B. Magnetic moments

We now turn to the problem of high-temperature ferromagnetism. First, in 5% doped (Sc, Ti,…,Cu, Zn) SnO_2 films (Fig. 12), the room temperature magnetism is only found for Cr, Mn, Fe, Co, and Ni. This is unlike in ZnO, prepared in similar conditions, where Ti, V, and even Sc (but not Mn) doping also results in high temperature ferromagnetism in ZnO.[4] Ferromagnetism is not linked to electrical conductivity. Only the Co-doped films are conducting for all dopant concentrations, whereas high concentrations of other dopants eventually lead to insulating films.

It is impossible to explain the large moments in Fig. 10 in terms of any known phases that might be present as impurities. Laying aside the lack of evidence for secondary phases, the pure metals Co and Fe have moments of 1.7 and 2.2 μ_B per atom, respectively. Concentrated transition-metal oxides normally exhibit antiferromagnetic superexchange interactions, which lead to antiferromagnetic or ferrimagnetic structures where the average moment per transition-metal cation does not exceed 1.5 μ_B. A few examples are Mn_3O_4, $T_C=43$ K which has a moment of 0.6 μ_B/Mn,[38] $SnMn_2O_4$ which is ferromagnetic, with $T_C=53$ K,[39] γ-Fe_2O_3 which is ferrimagnetic with $T_C=743$ K and a moment of 1.25 μ_B/Fe.[40] The data in Fig. 10 leave little doubt that the high-temperature ferromagnetism is an intrinsic property. It is quite implausible that ferromagnetic impurity phases could give rise to the same behavior in the Mn, Fe, and Co systems. In any case the moments at low concentrations far exceed those of all known ferromagnetic phases.

The variation of magnitude of the magnetic moment in SnO_2 shown in Fig. 10 can be partly explained in terms of the distribution of magnetic impurities in the rutile lattice. The idea is that isolated impurities possess the full spin-only moment on, but nearest-neighbor pairs are coupled antiferromagnetically, making no net contribution to the magnetization, triplets contribute $m/3$, quartets contribute zero and so on. The clusters are assumed to couple ferromagnetically. A calculation was carried out numerically by simulating a body-centered cubic lattice with 2×10^6 lattice sites, occupied at random. The result of the model shown by the dotted line in Fig. 10(a) compares favorably with the data.

The difficulty is the moments in excess of the spin-only values, first observed in $(Sn_{0.95}Co_{0.05})O_2$ by Ogale *et al.*,[8] which also appear at low doping levels in the present work. Allowing for likely uncertainty in thickness and composition, we find an average Mn moment for the lowest concentration $x=0.1\%$ of 20 ± 1 μ_B, which is to be compared with the spin-only value of 4 μ_B for Mn^{3+}. In no case, including that where orbital moments reside on the donor states, could the moment exceed $(5+\delta/x)$ μ_B per Mn. The spin moment on a ligand hole [Fig. 13(c)] could add at most 1 μ_B per 3*d* cation. The observed moments at low concentrations are inexplicable if the only source of magnetism in doped SnO_2 is the transition metal dopant.

The fact that all three dopants in Fig. 10 produce high-temperature ferromagnetism with roughly the same upturn in moment at low concentrations, means that the moment of the films is approximately constant, regardless of composition. Similarly, the moment is (very) approximately independent of film thickness (Fig. 11). A possible explanation for such behavior is the presence of magnetic centers in the doped SnO_2 films in the vicinity of the substrate/film interface which are not identified with the 3d cations. The idea that the interface play a role is supported by the observation that a ferromagnetic moment is observed when V-doped SnO_2 films are deposited by PLD on some substrates (eg. $LaAlO_3$) but not others (eg. Al_2O_3).[11] The thickness of the region in which the magnetic centers are located may be inferred from the fact that a 10 nm film of $(Sn_{0.95}Co_{0.05})O_2$ exhibits practically the full moment of 220 μ_B nm^{-2}. Furthermore, the moment is so large that it cannot be entirely located *at* the interface (1 nm^2 is the area occupied by about four SnO_2 formula units). Undoped SnO_2 films show no ferromagnetism. It therefore seems that the defect centers have a nonmagnetic ground state, but that a low-lying magnetic excited state is stabilized by exchange coupling to a 3*d* dopant ion[41] (Fig. 13). There is evidence of such a singlet/triplet structure for two-electron defects in other oxides.[42,43] In SnO_2, peroxide ions are candidates for the two-electron defect centers.

C. Exchange interactions

Carrier-mediated ferromagnetic exchange has to be effective whether or not the carriers are delocalized, as indicated by the semiconducting behavior of all the Co-doped samples and the Mn or Fe samples with less than 7% or 15% of transition metal, and the insulating behavior of the more highly-doped Mn and Fe materials. The interaction is long-range. It cannot be nearest-neighbor superexchange or double-exchange if the doping is uniform, because the doping level x in all the films is below the percolation threshold. For example, the cation nearest-neighbor distance is 0.37 nm whereas the average Mn-Mn distance in the $x=0.5\%$ Mn sample is 1.2 nm.

We explore three approaches to try to understand the exchange coupling and high Curie temperature. In model *A*, electrons in Bohr-like donor orbitals form magnetic polarons spanning several 3*d* dopant ions, and the magnetic polarons overlap to make a spin-split impurity band.[20] A variant of this is model *B*, where donor states lie close to the bottom of the 5*s* (Sn) conduction band, and feed a spin-split conduction band. In either case, the $3d^{\uparrow}$ levels lies in the $2p-5s$ gap. As originally proposed, our impurity band model for magnetic semiconductors identified the donor states providing *n*-type conductivity with oxygen vacancies (*F* centers) which form an impurity band that mediates the exchange between the dopant cations. The electrons associated with the singly-charged oxygen vacancies occupy *s*-like hydrogenic orbitals which may overlap to form an impurity band. This band is half filled with one electron per vacancy (the two electron per vacancy F' states lie much higher in energy and it can be spin polarized by exchange interaction with the 3*d* ions). In SnO_2, the defects giving rise to the conductivity are thought to be the sparse and easily-ionized Sn_i+V_o centers shown in Fig. 13(a); these defects can also form an impurity band, which mediates exchange.

The effective exchange between the 3*d* spins and the impurity band electrons in model *A* is

$$J_{sd}\mathbf{S}\,.\,\mathbf{s}|\psi(\mathbf{r})|^2\Omega,$$

where $|\psi(\mathbf{r})|^2$ is the electron density in the impurity band and Ω is the volume of the 3*d* shell, $\mathbf{S}$ the spin of the 3*d* cations which have volume Ω, and $\mathbf{s}$ is the donor electron spin. The *sd* exchange constant J_{sd} couples the 3*d* states to the electron density $|\psi(\mathbf{r})|^2$ in the impurity band. Developing the molecular field expression for the Curie temperature gives the result[20]

$$T_C=[S(S+1)s^2x\delta n/3]^{1/2}J_{sd}\omega_c/k_B,$$

where x is the atomic concentration of dopant cations. ω_c (typical value 6%) is the product of cation/anion volume ratio for the oxide and $\delta=n/n_O$ (n is the density of defects and n_O is the oxygen density $\approx 6\times 10^{28}$ m^{-3} for oxides with a close-packed oxygen lattice). If we take some typical values, $S=3/2$, $s=1/2$, $x=0.1$, $\delta=0.01$, $n=1$, $J_{sd}=1.5$ eV, $\omega_c=0.06$, we arrive at a value $T_C=18$ K. There is limited scope for increasing the Curie temperature in this model. The only way to increase T_C significantly is somehow increase the electron density $|\psi(\mathbf{r})|^2$ in the vicinity of the magnetic impurities. In order to transfer the necessary electrons from the donor states to each magnetic cation, empty 3*d* states should also lie close to the Fermi level, where they hybridize with the impurity band providing transfer of 0.01–0.02 electrons per cation from the impurity band to the 3*d* ion. Figure 12 suggests this process is most effective for Fe. The electrons in a narrow impurity band may be localized by random potential fluctuations due to the 3*d* ion impurities or by Coulomb interaction which produce a Mott-Hubbard splitting between the levels derived from singly or doubly-occupied *F* centers. Localization has no effect on the exchange interactions provided the localization length exceeds the polaron radius. The radius of the donor orbit for SnO_2 is $r_H=(\varepsilon m/m^*)a_0\approx 16a_0$ where ε, the high-frequency dielectric constant is 3.9, the Bohr radius $a_0=0.053$ nm and the effective mass of the carriers m^*/m is 0.24.[20]

In model *B*, the donors populate the spin-split conduction band. This is equivalent to the RKKY exchange interaction for low electron densities. The expression for T_C in the RKKY model for small values of $2k_Fr$ is[20]

$$T_C\approx zm^*S(S+1){J_{sd}}^2\delta({n^5x}/{{n_O}^2})^{1/3}(48\hbar^2k_B).$$

Substituting reasonable values, $J_{sd}=1.5$ eV, $z=12$, $S=5/2$, $n=1$, and $x=0.1$, $\delta=0.01$, we find $J_{RKKY}=0.23$ K, and $T_C=15$ K. This again is more than an order of magnitude too low. The way to increase T_C here is to augment the 4*s* character of the conduction band over the 5*s*. The random potential created by the 3*d* impurities can create a mobility edge at E_μ near the bottom of the the $4s/5s$ conduction band, which leads to a nonconducting ferromagnetic state when $E_F<E_\mu$.

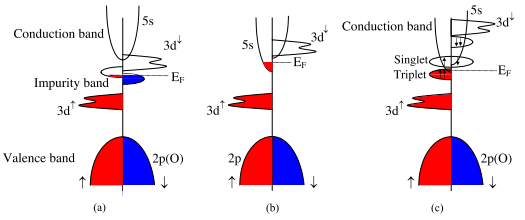

FIG. 14. (Color online) Different models for exchange discussed in the text. (a). Impurity band exchange (b). RKKY exchange (c). Two-electron defect-center exchange.

The predictions of the two models regarding the polarization of the states at the bottom of the conduction band are quite distinct. Model *A* predicts these states are ↓, for Fe, Co, or Ni while model *B* predicts they are ↑. A measurement of magnetic dichroism or spin-polarized photoemission may be able to resolve the question of the sign of the spin polarization at the Fermi level, and whether donor electrons mediating the exchange occupy a spin-split impurity band or a spin-split $4s/5s$ conduction band.

However, there must be a serious doubt whether either of these models tell the full story. The large discrepancy between the predicted and observed values of T_C, as well as the observation that only a fraction of the dopant cations is magnetically ordered[9,44] challenges the idea that the films are magnetically homogeneous. A tendency for the magnetic dopants to line up in threads or sheets could overcome the percolation problem, and the greater exchange energy density in the restricted magnetic regions would lead to higher Curie temperatures. Another problem is that the moment per dopant ion is atmost $(2S+x/\delta)\ \mu_B$, which is essentially the spin-only value. Larger moments might be explained if defects, which we supposed to be essentially electronic in nature, are involved more directly in the ferromagnetism.

This leads us to the third approach, model *C* where the defects have moments. In the simplest case, the moment of a two-hole defect involve a peroxide ion on two adjacent octahedral oxygen cages. More extended oxygen hole orbits can be envisaged, with lower percolation thresholds. The two-hole triplets can themselves form spin-split impurity band [Fig. 14(c)], in the same way as the hydrogenic donor or *F* center electrons. The extra spin moment introduced in this way can be no more than 1 μ_B per M^{3+} cation, but there is may be a possibility of an additional orbital moment depending on the symmetry of the defect state. The anisotropy of the susceptibility argues for a large orbital contribution. To account for much larger moments per $3d$ cation, the number of defects needs to be decoupled from the number of cations. Two-hole defects which are not induced by doping may be present at low $3d$ cation concentrations. These centers are not magnetic in undoped SnO_2, but they could be switched into a magnetic state by exchange coupling to a nearby $3d$ cation, as illustrated in Fig. 15. The extra moment arising in this way need not be limited to 1 μ_B per $3d$ cation.

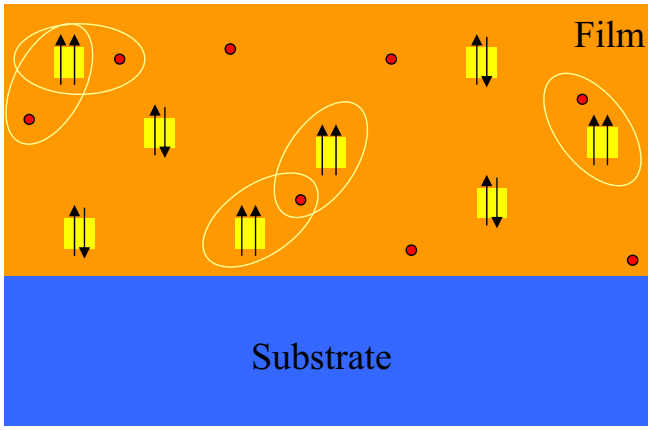

FIG. 15. (Color online) Illustration of the stabilization of two-electron/hole triplet states by coupling with magnetic dopant cations.

V. CONCLUSIONS

The high-temperature ferromagnetism in thin films of $(Sn_{1-x}M_x)O_2$ with M=Cr, Mn, Fe, Co, or Ni is an intrinsic effect. The moments at low concentrations approach or surpass the spin-only values, and they cannot be explained in terms of secondary impurity phases. Nor can the anisotropy of the magnetisation of the films be explained in these terms. Absence of anomalous Hall effect indicates that there is negligible $3d$ density of states at E_F.

Exchange, if it is mediated by donor electrons, acts in a way that seems to be equally effective whether the electrons are localized or delocalized. The exchange interactions need to be enhanced by more than an order of magnitude over the values applicable in a simple model of a magnetic polaron impurity band, or an RKKY-type interaction in the conduction band. This requires that the $3d^{\downarrow}$ states are also present at the Fermi level in the first case, and that the $4s$ (M) states lie below the $5s$ (Sn) states in the second case. These models differ in the sign of the spin polarization at the Fermi level.

Much of the magnetic moment, however, is associated with electronic defects or lattice defects, which are already present in the thinnest films. The dopants somehow serve to activate the defect moment, since the undoped films of SnO_2 are not ferromagnetic. The high Curie temperature observed for low dopant or defect levels ($\sim$1%) imply that the defect-related magnetism is inhomogeneous—it might be associated with grain boundaries for example—or else a new, long-range magnetic coupling mechanism must be found.

ACKNOWLEDGMENTS

This work forms part of the CINSE project funded by Science Foundation Ireland. L.S. Dorneles is supported by the Irish Research Council for Science, Engineering, and Technology.

[1] Y. Matsumoto, M. Murakami, T. Shono, T. Hasegawa, T. Fukumura, M. Kawasaki, P. Ahmet, T. Chikyow, S. Koshihara, and H. Koinuma, Science **291**, 854 (2001).
[2] Z. Wang, W. Wang and J. Tang, L. D. Tung, L. Spinu, and W. Zhou, Appl. Phys. Lett. **83**, 518 (2003).
[3] K. Ueda, H. Tabata, and T. Kawai, Appl. Phys. Lett. **79**, 988 (2001).
[4] M. Venkatesan, C. B. Fitzgerald, J. G. Lunney, and J. M. D. Coey, Phys. Rev. Lett. **93**, 177206 (2004).
[5] H. Saeki, H. Tabata, and T. Kawai, Solid State Commun. **120**, 439 (2001).
[6] P. Sharma, A. Gupta, K. V. Rao, F. J. Owens, R. Sharma, R. Ahuja, J. M. Osorio Guillen, B. Johansson, and G. A. Gehring, Nat. Mater. **2**, 673 (2003).
[7] D. B. Buchholz, R. P. H. Chang, J. H. Song, and J. B. Ketterson, Appl. Phys. Lett. **87**, 082504 (2005).
[8] S. B. Ogale, R. J. Choudhary, J. P. Buban, S. E. Lofland, S. R. Shinde, S. N. Kale, V. N. Kulkarni, J. Higgins, C. Lanci, J. R. Simpson, N. D. Browning, S. Das Sarma, H. D. Drew, R. L. Greene, and T. Venkatesan, Phys. Rev. Lett. **91**, 077205 (2003).
[9] J. M. D. Coey, A. P. Douvalis, C. B. Fitzgerald, and M. Venkatesan, Appl. Phys. Lett. **84**, 1332 (2004).
[10] N. H. Hong, J. Sakai, W. Prellier, and A. Hassini, J. Phys.: Condens. Matter **17**, 1697 (2005).
[11] N. H. Hong and J. Sakai, Physica B **358**, 265 (2005).
[12] N. H. Hong, J. Sakai, N. T. Huong, N. Poirot, and A. Ruyter, Phys. Rev. B **72**, 045336 (2005); N. H. Hong, A. Ruyter, W. Prellier, J. Sakai, and N. T. Huong, J. Phys.: Condens. Matter **17**, 6533 (2005).
[13] S. Sonoda, S. Shimizu, T. Sasaki, Y. Yamamoto, and H. Hori, J. Cryst. Growth **237**, 1358 (2002).
[14] D. Kumar, J. Antifakos, M. G. Blamire, and Z. H. Barber, Appl. Phys. Lett. **84**, 5004 (2004).
[15] C. Liu, F. Yun, and H. Morkoç, J. Mater. Sci.: Mater. Electron. **16**, 555 (2005).
[16] C. B. Fitzgerald, M. Venkatesan, J. G. Lunney, L. S. Dorneles, and J. M. D. Coey, Appl. Surf. Sci. **247**, 493 (2005).
[17] A. M. Nazmul, S. Sugahara, and M. Tanaka, Phys. Rev. B **67**, 241308(R) (2003).
[18] T. Dietl, Semicond. Sci. Technol. **17**, 377 (2002).
[19] A. Kaminski and S. Das Sarma, Phys. Rev. Lett. **88**, 247202 (2002).
[20] J. M. D. Coey, M. Venkatesan, and C. B. Fitzgerald, Nat. Mater. **4**, 173 (2005).
[21] J. Y. Kim, J. H. Park, B. G. Park, H. J. Noh, S. J. Oh, J. S. Yang, D. H. Kim, S. D. Bu, T. W. Noh, H. J. Lin, H. H. Hsieh, and C. T. Chen, Phys. Rev. Lett. **90**, 017401 (2003).
[22] S. A. Chambers, S. Thevuthasan, R. F. C. Farrow, R. F. Marks, J. U. Thiele, L. Folks, M. G. Samant, A. J. Kellock, N. Ruzycki, D. L. Ederer, and U. Diebold, Appl. Phys. Lett. **79**, 3467 (2001).
[23] S. R. Shinde, S. B. Ogale, J. S. Higgins, H. Zheng, A. J. Millis, V. N. Kulkarni, R. Ramesh, R. L. Greene, and T. Venkatesan, Phys. Rev. Lett. **92**, 166601 (2004).
[24] D. P. Norton, S. J. Pearton, A. F. Hebard, N. Theodoropoulou *et al.*, Appl. Phys. Lett. **82**, 239 (2003).
[25] K. Rode, A. Anane, R. Mattana, J. P. Contuor *et al.*, J. Appl. Phys. **93**, 7676 (2003).
[26] S. Ramachandran, A. Tiwari, and J. Narayan, Appl. Phys. Lett. **84**, 5255 (2004).
[27] K. J. Kim and Y. R. Park, Appl. Phys. Lett. **81**, 1420 (2001).
[28] D. A. Schwartz, N. S. Norberg, Q. P. Nguyen, J. M. Parker, and D. M. Gamelin, J. Am. Chem. Soc. **125**, 13205 (2003).
[29] A. C. Tuan, J. D. Bryan, A. B. Pakhomov, V. Shutthanandan, S. Thevuthasan, D. E. McCready, D. Gaspar, M. H. Engelhard, J. W. Rogers, K. Krishnan, D. R. Gamelin, and S. A. Chambers, Phys. Rev. B **70**, 054424 (2004).
[30] J. Okabayashi, K. Ono, M. Mizuguchi, M. Oshima, Subhra Sen Gupta, D. D. Sarma, T. Mizokawa, A. Fujimori, M. Yuri, C. T. Chen, T. Fukumura, M. Kawasaki, and H. Koinuma, J. Appl. Phys. **95**, 3573 (2004).
[31] H. Kimura *et al.*, Appl. Phys. Lett. **80**, 94 (2002).
[32] C. Kilic and A. Zunger, Phys. Rev. Lett. **88**, 095501 (2002).
[33] T. Kasuya, Solid State Commun. **8**, 1635 (1970).
[34] C. B. Fitzgerald, M. Venkatesan, A. P. Douvalis, S. Huber, J. M. D. Coey, and T. Bakas, J. Appl. Phys. **95**, 7390 (2004).
[35] L. S. Dorneles, D. O'Mahony, C. B. Fitzgerald, F. McGee, M. Venkatesan, I. Stanca, J. G. Lunney, and J. M. D. Coey, Appl. Surf. Sci. **248**, 406 (2005).
[36] L. R. Doolittle, Nucl. Instrum. Methods Phys. Res. B **9**, 344 (1985).
[37] A. Tarre, A. Rosental, J. Sundqvist, A. Hårsta, T. Uustare, and V. Sammelselg, Surf. Sci. **532**, 514 (2003).
[38] K. Dwight and N. Menyuk, Phys. Rev. **119**, 1470 (1960).
[39] D. G. Wickham, N. Menuyk, and K. Dwight, J. Phys. Chem. Solids **20**, 316 (1961).
[40] H. Takei and S. Chiba, J. Phys. Soc. Jpn. **21**, 1255 (1966).
[41] J. M. D. Coey, J. Appl. Phys. **97**, 10D313 (2005).
[42] A. M. Stoneham, *Theory of Defects in Solids*, Chap. 16 (Clarendon Press, Oxford, 1975).
[43] A. M. Stoneham, A. P. Pathak, and R. H. Bartram, J. Phys. C **9**, 73 (1976).
[44] A. Punnoose, J. Hays, A. Thurber, M. H. Engelhard, R. K. Kukkadapu, C. Wang, V. Shutthanandan, and S. Thevuthasan, Phys. Rev. B **72**, 054402 (2005).